

PL-TR-97-2082

**DESIGN, DEVELOP, FABRICATE, TEST
AND DELIVER A PROTOFLIGHT
MEDIUM-TO-HIGH-ENERGY ELECTRON
DETECTOR FOR INTEGRATION
INTO A SMALL ON-BOARD DIAGNOSTIC
SENSORS PACKAGE**

**Jeffrey E. Belue
Frederick A. Hanser
Paul R. Morel**

**PANAMETRICS, INC.
221 Crescent Street
Waltham, MA 02154-3497**

16 June 1997

Scientific Report No. 1

Approved for public release; distribution unlimited

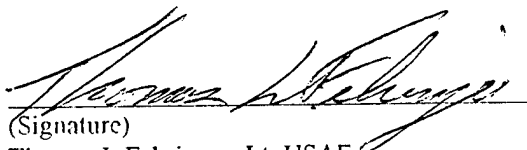
DTIC QUALITY INSPECTED 6

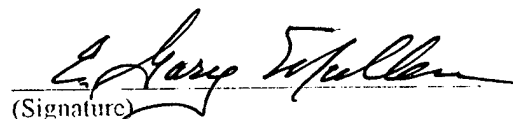


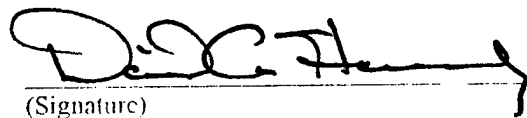
**PHILLIPS LABORATORY
Directorate of Geophysics
AIR FORCE MATERIEL COMMAND
HANSCOM AFB, MA 01731-3010**

19970819 029

This Scientific Report #1 has been reviewed and is approved for publication.


(Signature)
Thomas L. Fehringer, Lt. USAF
Contract Manager


(Signature)
E. Gary Mullen
Branch Chief


(Signature)
David Hardy
Division Director

This report has been reviewed by the ESC Public Affairs Office (PA) and is releasable to the National Technical Information Service (NTIS).

Qualified requestors may obtain additional copies from the Defense Technical Information Center (DTIC). All others should apply to the National Technical Information Service (NTIS).

If your address has changed, if you wish to be removed from the mailing list, or if the addressee is no longer employed by your organization, please notify PL/IM, 29 Randolph Road, Hanscom AFB, MA 01731-3010. This will assist us in maintaining a current mailing list.

Do not return copies of this report unless contractual obligations or notices on a specific document require that it be returned.

REPORT DOCUMENTATION PAGE			Form Approved OMB No. 0704-0188	
<small>Public reporting burden for this collection of information is estimated to average 1 hour per response, including the time for reviewing instructions, searching existing data sources, gathering and maintaining the data needed, and completing and reviewing the collection of information. Send comments regarding this burden estimate or any other aspect of this collection of information, including suggestions for reducing this burden, to Washington Headquarters Services, Directorate for Information Operations and Reports, 1215 Jefferson Davis Highway, Suite 1204, Arlington, VA 22202-4302, and to the Office of Management and Budget, Paperwork Reduction Project (0704-0188), Washington, DC 20503.</small>				
1. AGENCY USE ONLY (Leave blank)		2. REPORT DATE 16 June 1997	3. REPORT TYPE AND DATES COVERED Scientific No. 1	
4. TITLE AND SUBTITLE Design, Develop, Fabricate, Test and Deliver a Protoflight Medium-to-High-Energy Electron Detector for Integration Into a Small On-Board Diagnostic Sensors Package			5. FUNDING NUMBERS Contract Number: F19628-95-C-0196 PE 63410F PR 2822 TA GC WU PM	
6. AUTHOR(S) Jeffrey E. Belue, Frederick A. Hanser, Paul R. Morel				
7. PERFORMING ORGANIZATION NAME(S) AND ADDRESS(ES) Panametrics, Inc. 221 Crescent Street Waltham, MA 02154-3497			8. PERFORMING ORGANIZATION REPORT NUMBER	
9. SPONSORING / MONITORING AGENCY NAME(S) AND ADDRESS(ES) Phillips Laboratory 29 Randolph Road Hanscom AFB, MA 01731-3010 Contract Monitor: Lt. Thomas Fehringer/GPSH			10. SPONSORING / MONITORING AGENCY REPORT NUMBER PL-TR-97-2082	
11. SUPPLEMENTARY NOTES				
12a. DISTRIBUTION / AVAILABILITY STATEMENT Approved for public release; Distribution unlimited.			12b. DISTRIBUTION CODE	
13. ABSTRACT (Maximum 200 words) An electron spectrometer is being designed to measure electron flux in the range of 3 to 30 MeV. A breadboard unit has been designed and tested, using a solid state detector telescope for geometric factor definition and a Cerenkov radiator/PMT for energy measurement. The measured response to electrons is very broad, so the Cerenkov radiator is being redesigned as a larger volume with larger PMTs to improve the energy resolution. Following testing of the modified Cerenkov radiator/PMT, a protoflight unit will be fabricated, tested and calibrated. The protoflight electron spectrometer is to be integrated to the Small Onboard Environmental Diagnostic Sensors (SOBEDS) Package.				
14. SUBJECT TERMS Electron Detector Electron Flux Cerenkov Detector Proton Flux Electron Spectrometer Space Radiation			15. NUMBER OF PAGES 26	
			16. PRICE CODE	
17. SECURITY CLASSIFICATION OF REPORT UNCLASSIFIED	18. SECURITY CLASSIFICATION OF THIS PAGE UNCLASSIFIED	19. SECURITY CLASSIFICATION OF ABSTRACT UNCLASSIFIED	20. LIMITATION OF ABSTRACT UNLIMITED	

Table of Contents

1.0 Introduction	1
2.0 Sensor Design, Analysis, and Test Results	2
2.1 Conceptual Design	2
2.2 Breadboard Detector	8
2.3 Analog Signal Processing Electronics	8
2.4 Digital Electronics	9
2.3 Breadboard Calibration Data Analysis	11
2.3.1 Atmospheric Muon Test Results	11
2.3.2 Proton Tests at the Harvard Cyclotron	11
2.3.3 Electron Tests at the RPI Linear Accelerator	11
3.0 Preliminary Design Review	17
3.1 Electronics Design Issues	17
3.1.1 Low Voltage DC to DC Converter	17
3.1.2 Standby Power and Power-On Current	18
3.1.3 Electronic Parts Issues	18
3.2 Measured Electron Energy Resolution	18
4.0 Sensor Design Status	18
4.1 Analog Signal Processing	19
4.2 High Voltage Power Supply	19
4.3 Digital Processing	19
4.4 Mass, Power	19
4.5 Spacecraft Interface	19
5.0 Future Work	19
References	21

List of Figures

<u>Figure</u>	<u>Page</u>
1 Initial Spectrometer Outline Drawing	1
2 Initial Detector Geometry	3
3 Ionization Energy Loss in the Detectors	3
4 Cerenkov Light Production in the Radiator	5
5 Spectrometer Electronics Block Diagram	7
6 Breadboard Detector Assembly	9
7 Cerenkov Radiator Design	10
8 Digital Processing FPGA	12
9 Electron Area(0°) Response, Near Station	13
10 Electron Geometric Factor Response, Near Station	14
11 Electron Area Response, Far Station	15
12 Electron Geometric Factor Response, Far Station	16
13 Electron Area Response, with Pile-up at Near Station	16
14 Electron Respose vs. Electron Energy	17

List of Tables

<u>Table</u>	<u>Page</u>
1 SSD Energy Loss Threshold Values	6
2 Cerenkov Light Thresholds and Particle Energies	6
3 Summary of Measured Detector Areas(0°)	13
4 Summary of Measured Geometric Factors	14
5 Proposed Spectrometer Telemetry Packet	20
6 Spectrometer Summary of Characteristics	21

1.0 Introduction

High energy electron flux is a very important radiation hazard to spacecraft electronics. Measurement of electron flux along with its variation in time and position across the magnetosphere allows a quantitative understanding of the radiation hazard. The goal of the work described in this report is to design a sensor that measures the high energy electron flux.

A satellite sensor to detect 3 to 30 MeV electrons is being designed and developed. The sensor uses three solid state detectors (SSDs) and a quartz Cerenkov radiator. Two SSDs in a telescope configuration form a 9° FWHM detection cone, while the Cerenkov radiator performs the particle energy measurement. The third SSD is behind the Cerenkov radiator, and discriminates electrons from relativistic protons. A fast triple coincidence of the two telescope SSDs and the Cerenkov detector initiates particle analysis. A microcontroller analyzes the detector outputs and stores the counts in a seven-channel electron energy spectrum. Shielding is designed to reduce background count rates in the detectors to minimize random triple coincidences. The design is applicable to spacecraft in the earth's trapped radiation belts, with the electronics design being hard to >100 kRad. A breadboard sensor and a protoflight sensor are to be designed, fabricated, calibrated, and tested, with the protoflight sensor being delivered for possible flight. The initial spectrometer outline drawing is shown in Figure 1.

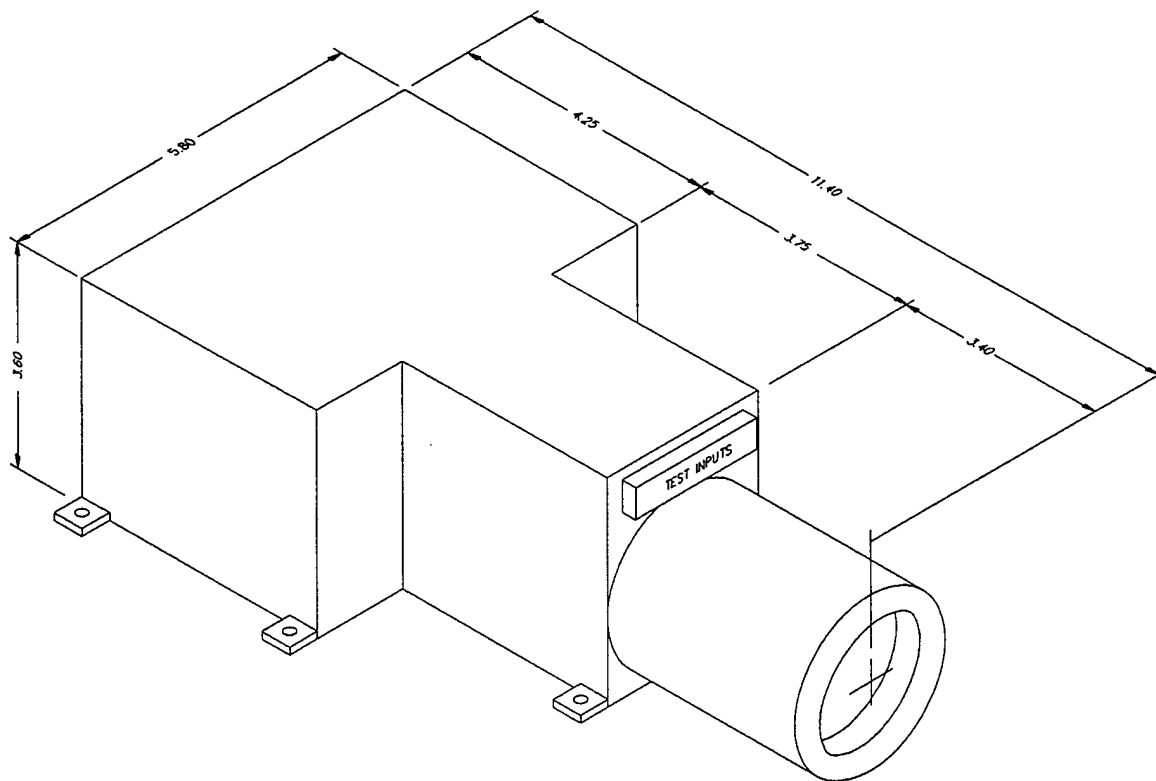


Figure 1 Initial Spectrometer Outline Drawing.

A breadboard unit has been designed, fabricated, and calibrated with protons and electrons. The low energy proton response is negligible, so non-penetrating protons will not contaminate the electron spectrum. However, the initial breadboard Cerenkov radiator design has a very broad energy response for electrons, and the design is being upgraded to provide better energy resolution. The breadboard design, analysis, and test results are described in Section 2.0. The results of an informal Preliminary Design Review are discussed in Section 3.0, while the current status of the sensor design is given in Section 4.0. Future work is discussed briefly in Section 5.0, and at present is being confined to upgrading the Cerenkov detector design to give better electron energy resolution and verifying this with electron beam calibration.

2.0 Sensor Design, Analysis, and Test Results

2.1 Conceptual Design

The initial detector geometry is shown in Figure 2. A telescope arrangement of two solid state detectors (SSDs, D1 and D2) is used to define the sensor field-of-view (FOV), with a 2.5-inch thick quartz Cerenkov radiator providing electron energy selection. A third SSD (D3), behind the Cerenkov radiator, provides discrimination between electrons and high energy penetrating protons. D1 and D2 are 700 micron thick, 2 cm² area totally depleted Si surface barrier detectors. The separation is 3.75 inches, which produces a geometric factor of 0.044 cm²-sr with a maximum off-axis detection angle of 9.5°. The front collimator extension is used to reduce the D1 geometric factor for lower energy electrons and thus avoid excessive count rates. A 46 mil Be foil is used to shield D1 from electrons below 0.5 MeV in the FOV. The Cerenkov radiator is 2.5-inch thick quartz, which is the range thickness for 31.76 MeV electrons and 125.5 MeV protons. The Cerenkov radiator has a 1-inch square entrance face and a 1.5-inch diameter (square for the breadboard design) rear face. Four sides are tapered flat from front to rear, and the design is such that all particles in the D1/D2 telescope FOV must pass completely through the radiator. Two ruggedized photomultiplier tubes (PMTs) are mounted on two of the flat side sections of the radiator, with the remaining area of the radiator being covered with white reflective paint. D3 is a 500 micron partially depleted, 20 cm² area Si detector, which covers the entire D1/D2 telescope FOV.

The calculated ionization energy loss in the SSDs and the Cerenkov radiator is shown in Figure 3, while the calculated Cerenkov light produced is shown in Figure 4. These calculations are used to provide the threshold values needed to produce the desired electron energy channels. D1 and D2 have nearly identical responses to electrons (>1 MeV) and protons (>350 MeV) which produce Cerenkov light in the quartz radiator, since the particles are all near the minimum ionization energy loss of 1.5 - 2 MeV-cm²/g in Si. This is shown in Figure 3, which shows the energy loss for electrons and protons in the three SSDs and in the Cerenkov radiator. The energy losses are calculated from the electron tables of Ref. 1 and 2, and the proton tables of Refs. 3 and 4. Note that the particle energy loss in the Cerenkov radiator should not produce any light, since pure quartz (fused silica) has an extremely low scintillation efficiency.

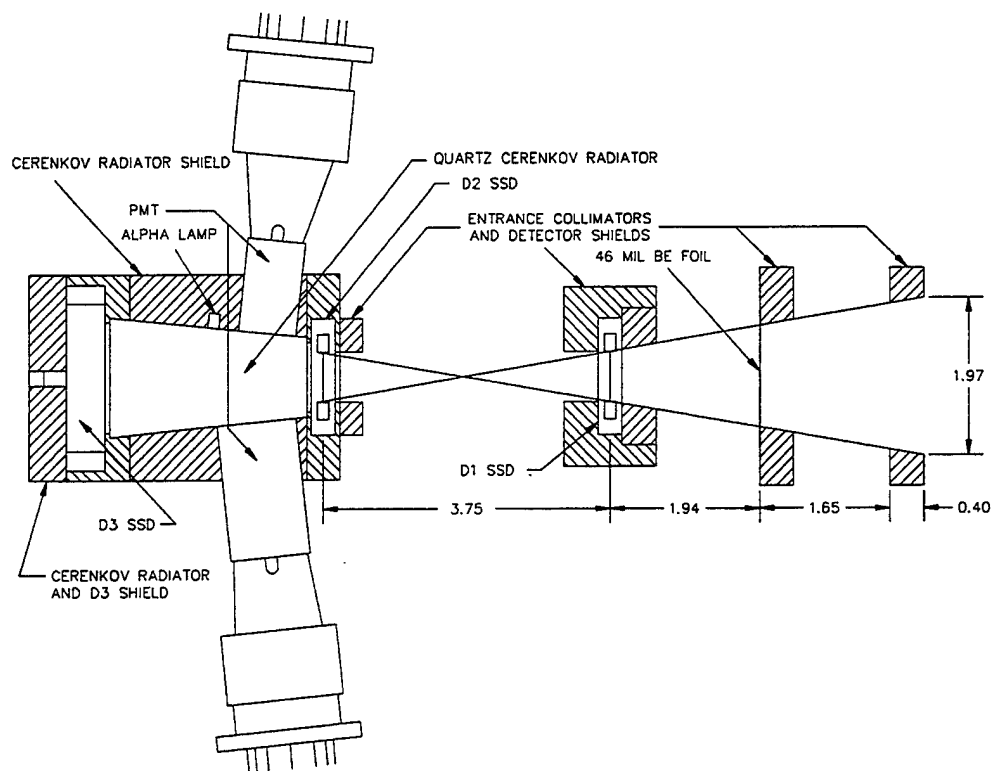


Figure 2 Initial Detector Geometry.

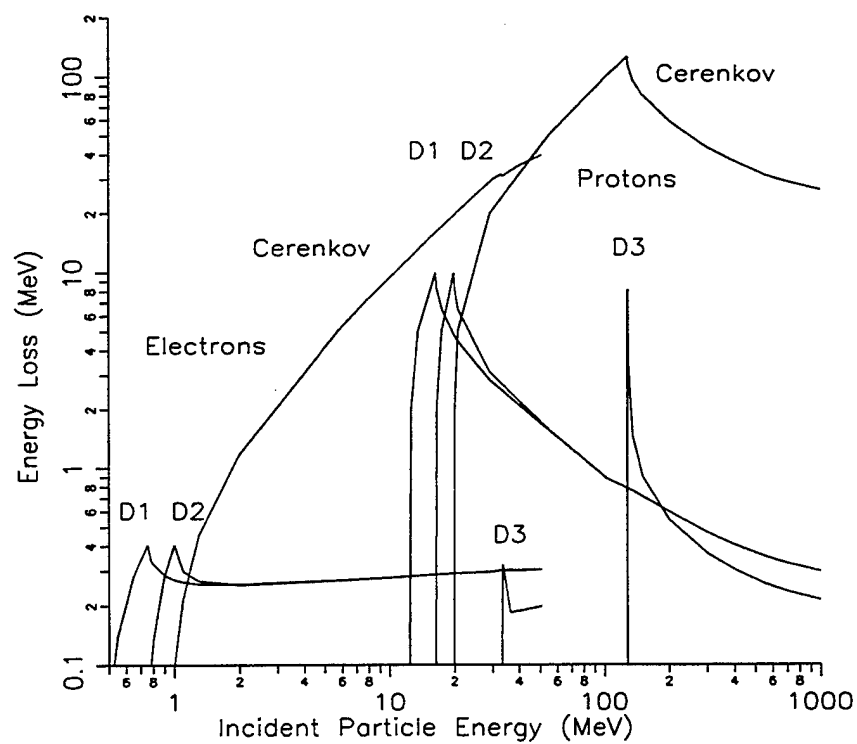


Figure 3 Ionization Energy Loss in the Detectors.

Particle energy discrimination comes from the Cerenkov light output of the radiator, with electron/proton selection coming from D3. The Cerenkov light produced in quartz is (Ref. 5)

$$d^2N/(dx dv) = K (1 - 1/(n\beta)^2) \text{ photons}/(\text{cm} \cdot (\text{cycles/s})) \quad (2.1)$$

where

$$K = 2\pi z^2/(137c), \quad \beta = v/c \quad (2.2)$$

with z the particle charge (in electron charges), v the particle velocity (cm/s), $c = 3 \times 10^{10}$ cm/s is the speed of light, and n is the index of refraction ($= 1.49$ for quartz). For a particle of kinetic energy E and rest mass $E_0 = mc^2$,

$$\beta^2 = (E^2 + 2EE_0)/(E + E_0)^2 \quad (2.3)$$

while the inverse is

$$E = E_0(1/(1 - \beta^2)^{1/2} - 1) \quad (2.4)$$

The minimum energy for Cerenkov light production is for $\beta_m = 1/n$, so for quartz the electron Cerenkov light threshold ($m_e c^2 = 0.511$ MeV) is 0.178 MeV, and for protons ($m_p c^2 = 938.3$ MeV) it is 327.4 MeV. The stopping power of quartz ($S(E)$ in MeV-cm²/g) is given for protons in Ref. 3, while for electrons it must be calculated from the Si stopping power in Ref. 2 and the O stopping power in Ref. 1 using the mass fractions of the elements in quartz (SiO₂). Using the energy loss per cm, $dE/dx = -\rho S(E)$ where $\rho = 2.20$ g/cm³ is the density of quartz, and converting (2.1) to wavelength λ by $dv = -cd\lambda/\lambda^2$, the PMT photoelectron yield can be written as

$$N_{pe} = \int (QE(\lambda)/\lambda^2) d\lambda \times \int_{E_m}^{E_i} [Kc(1 - 1/(n\beta)^2)/(\rho S(E))] dE \quad (2.5)$$

where E_m is the Cerenkov threshold energy and E_i is the energy of the particle when it enters the Cerenkov radiator. $QE(\lambda)$ is the fractional quantum efficiency of the PMT photocathode. The preliminary ruggedized PMT selected has a bialkali photocathode and a borosilicate glass face, giving a response range of 300 to 650 nm with a peak QE of about 0.27 (27%), which gives $\int (QE(\lambda)/\lambda^2) d\lambda = 3520/\text{cm}$.

The integration over electron and proton energy in (2.5) was done numerically, using the appropriate range/energy table, to calculate $N_{pe}(E_i)$ for several values of E_i . Note that N_{pe} from (2.5) is for complete light collection, and the actual value is expected to be about half of the (2.5) values. For the geometry of Figure 2 the light collection efficiency can be written approximately as

$$L_{ce} = f_A/[1 - (1 - f_A) \times R] \quad (2.6)$$

where $f_A \approx 0.0358$ is the ratio of total photocathode area (2 PMTs) to the total surface area of the Cerenkov radiator, and R is the reflectivity of the white paint. For $R = 0.95$, $L_{ce} = 0.43$, while for $R = 0.98$ (possible with a very high quality BaSO₄ coating), $L_{ce} = 0.65$. Using a reasonable estimate of $L_{ce} = 0.5$, a 2.21 MeV electron (corresponding to a 3 MeV incident electron) should produce a signal of about 21 actual photoelectrons, and this is definitely

detectable with good quality PMTs. This corresponds to a proton energy threshold of 369 MeV (371 MeV incident energy), so it is also possible to measure proton energy spectra from 371 MeV to above 1000 MeV.

The E_i values of (2.5) for particles in the FOV must be adjusted for the energy loss in the two telescope SSDs and in the 46 mil Be foil to give an E_{i0} value for the incident particle energy. The results for electrons and protons are shown in Figure 3. Since electrons below 31.76 MeV do not penetrate the Cerenkov radiator, they do not produce a D3 pulse, while all protons producing a Cerenkov signal must produce a D3 signal. Thus the D3 signal is used to distinguish electrons from protons.

The calculated electron energy losses and Cerenkov light outputs assume a straight line path for the electrons. Because of scattering the actual electron paths are irregular, and thus some electrons above the 31.76 MeV Cerenkov radiator thickness range will still stop within the radiator. The sensor will thus have some reduced response to higher energy electrons, and may be useable for electrons up to 40 MeV.

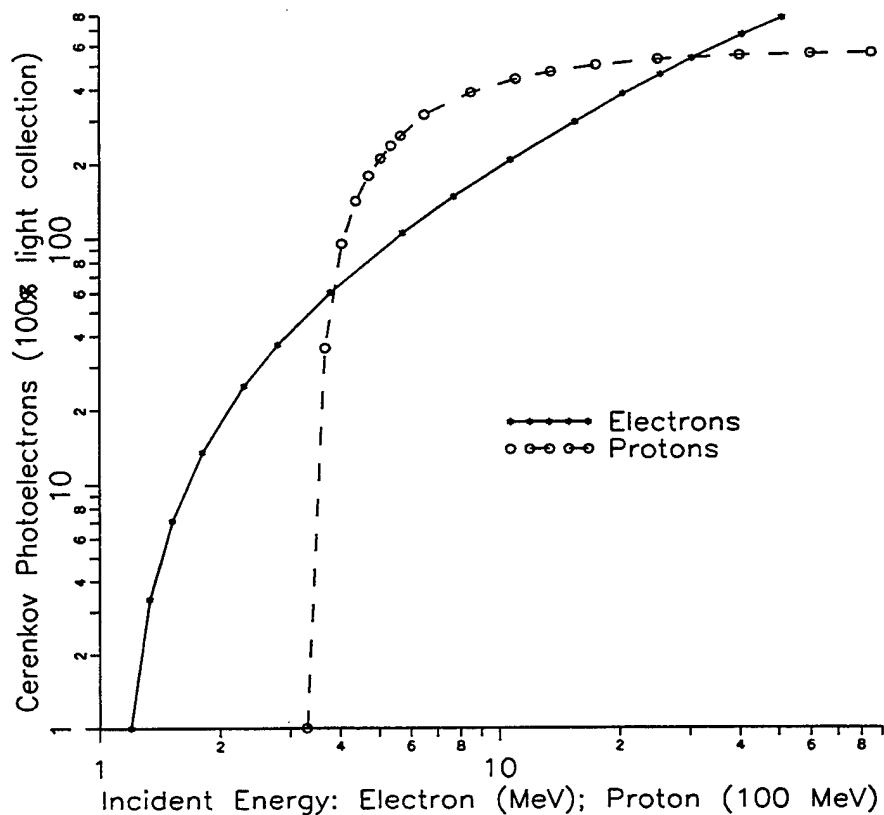


Figure 4 Cerenkov Light Production in the Radiator.

A preliminary set of SSD thresholds is given in Table 1 along with the corresponding incident electron and proton energies. The Cerenkov pulse spectrum is sorted into 8 levels, with the corresponding electron and proton energies being listed in Table 2. The energies in

Table 2 are nominal calculations, and in practice will be replaced with calibrated values obtained from actual electron calibration data. Electron (no D3(LL)) and proton (with D3(LL)) spectra are generated by a fast triple coincidence of D1(LL) + D2(LL) + PMT(LL) ($\tau = 0.1 \mu\text{s}$ resolving time), with the energy sorting by PMT(Li). Spectra are only taken for D1 and D2 energy losses in the range of LL to UL, which eliminates possible low energy proton contamination (protons $< 275 \text{ MeV}$). All thresholds are counted, providing several additional counts which allow correction of the measured data for deadtime and random coincidence effects.

Table 1 SSD Energy Loss Threshold Values				
Detector	Level	Value (MeV)	Particle Energy (MeV)	
			Electrons	Protons
D1	LL	0.13	>0.54	>12.35
"	UL	0.5	-	12.40 - 275
D1	LL	0.13	>0.80	>16.36
"	UL	0.5	-	16.41 - 275
D3	LL	0.13	>33.3	>128

Table 2 Cerenkov Light Thresholds and Particle Energies			
Cerenkov Level	Calculated Photoelectrons	Particle Energy (MeV)	
		Electrons	Protons
LL	41.6	3.0	371
L1	74.8	4.4	391
L2	149.6	7.8	445
L3	224	11.7	522
L4	299	15.8	626
L5	374	20.	812
L6	449	25.	1179
L7	523	30.	2431

The initial electronics block diagram is shown in Figure 5. The two front SSD (D1 and D2) output signals are amplified and shaped then the signal is applied to two threshold discriminators (TH/OSs) and a zero cross sensor (Z/C). The PMT output signals are summed, amplified and shaped then applied to a low level threshold discriminator (TH/OS), a zero cross sensor (Z/C) and an array of seven additional threshold discriminators (TH/OS). The rear SSD (D3) output signal is amplified and shaped then applied to a single threshold discriminator (TH/OS).

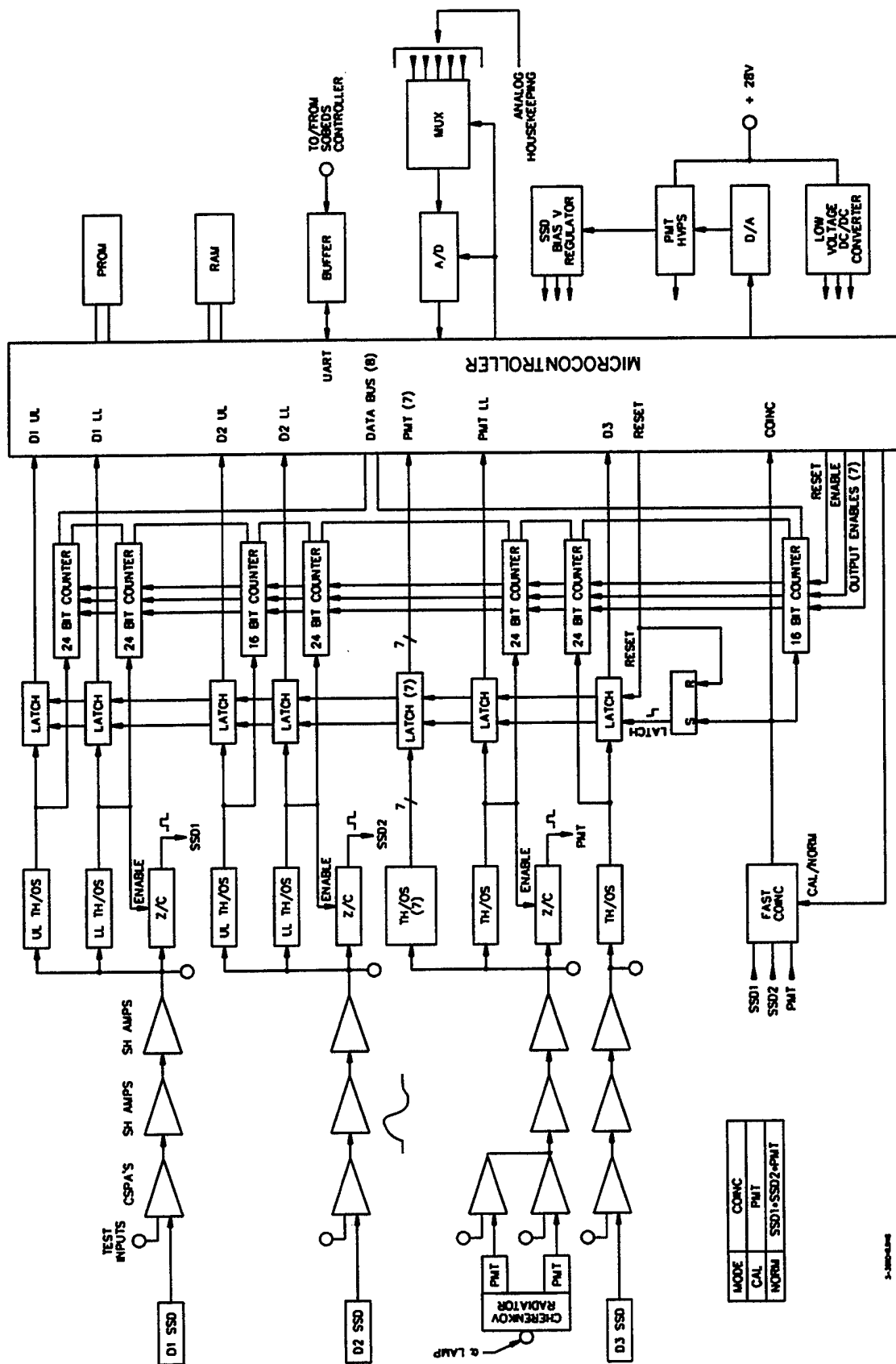


Figure 5 Spectrometer Electronics Block Diagram.

Incident electrons greater than 3.0 MeV within the FOV trigger the D1, D2 and PMT zero cross sensors, yielding a fast coincidence (FAST COINC) output pulse (COINC). Incident protons greater than 371 MeV within the FOV also trigger the D1, D2 and PMT zero cross sensors; however, these particles also trigger the rear SSD (D3) threshold (TH/OS). The COINC pulse latches the state of the SSD and PMT TH/OSs and interrupts the microcontroller; which reads and resets the latches, and increments a random access memory (RAM) based COINC pulse counter. Based on the state of the latches, the microcontroller also increments one of an array of RAM based counters. The microcontroller then returns to its background processing task, until it is again interrupted by a COINC pulse. Thus, seven differential channel and one integral channel energy analyses of electrons from 3.0 to >30. MeV, and of protons from 371 to >2431 MeV are performed. The SSD and PMT TH/OS and FAST COINC output pulses are also accumulated in hardware counters, which are periodically read and reset by the microcontroller in order to establish a dead time correction factor.

It is anticipated that data packets will be transferred to the Small Onboard Environmental Diagnostic Sensors (SOBEDS) Package central processing unit via a buffered universal asynchronous receiver/transmitter (UART). The Spectrometer microcontroller will format the Spectrometer data in a packet structure defined by the SOBEDs interface.

2.2 Breadboard Detector

Design, fabrication, and functional testing of the initial breadboard detector assembly was completed. The breadboard detector assembly is housed in a standard steel NEMA electrical enclosure, as shown in Figure 6. The breadboard Cerenkov radiator is a truncated, square pyramid, as shown in Figure 7. This design allows measurement of the collection efficiency with different PMT photocathode areas and locations on the radiator surface. The final Cerenkov radiator design may be modified to improve the light collection efficiency once the final PMT configuration is established.

The initial detector array design consisted of two PMT's (PMT1=0.75" and PMT2=1" diameter photocathodes), and two SSD's. Note that the PMT's can be mounted at the front or rear of the Cerenkov radiator during testing. Testing was done at Panametrics using radioactive sources and atmospheric muons; at the Harvard Cyclotron for protons; and at the Rensselaer Polytechnic Institute (RPI) Linear Accelerator, in Troy NY, for electrons.

2.3 Analog Signal Processing Electronics

The initial signal processing electronics consisted of the D1, D2, and PMT charge sensitive preamplifiers (CSPAs), shaping amplifiers (SH AMPS), threshold discriminators/one shots (TH/OSs) and zero-cross sensors (Z/Cs). This electronics breadboard was thoroughly tested, including temperature testing from -55 °C to +125 °C.

Each of the functional blocks, titled TH/OS in Figure 5, consists of an analog threshold (TH) discriminator whose output is input to a timing element called a one shot (OS). The one shot provides critical timing that is generally designed with discrete hardware (monostable multivibrator) for each TH/OS functional block. A circuit was designed to use a single FPGA to implement the one shot function, digitally, multiple times. Since seven different analog signal paths require the one shot function, the FPGA use saves a significant amount of Printed Circuit Board (PCB) space. Reducing PCB space helps to keep the overall spectrometer

package size small, and reduces instrument mass. Fast coincidence logic was also designed into the same FPGA.

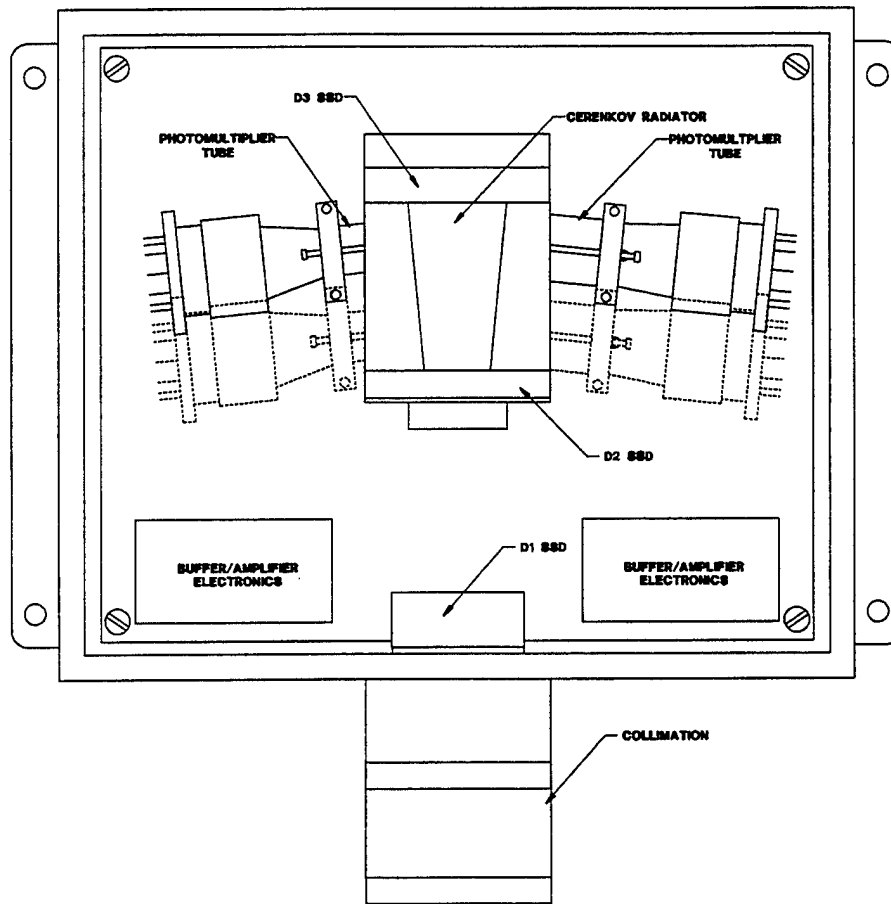


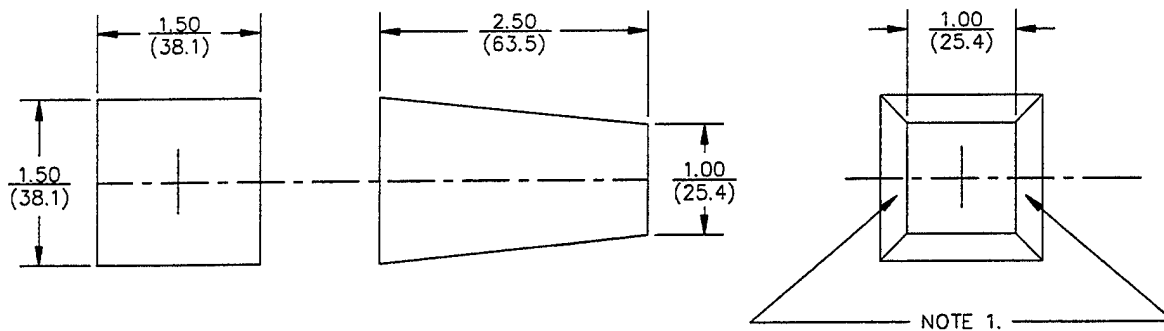
Figure 6 Breadboard Detector Assembly.

2.4 Digital Electronics

The digital electronics consists of the latches and counters that interface to the analog discriminators and the microcontroller (μC) with its associated support, including the spacecraft interface. The baseline design uses an industry standard microcontroller architecture, Intel's 8XC51FC, manufactured by United Technologies Microelectronics Center (UTMC), UT69RH051, which is radiation hard to a total dose of 1×10^6 rad and is latch-up immune. The microcontroller internal features include:

- * Three programmable 16-bit timer/counters
- * Internal clock/oscillator, of static design, controlled by an external crystal
- * 256 bytes of on-chip [internal] Read/Write Memory
- * Industry standard MCS®-51 instruction set
- * 64k of external program and data memory space
- * Universal asynchronous receiver/transmitter (UART)

The microcontroller executes its program from external rad-hard non-volatile PROM. Since the μC operates out of PROM, unambiguous program operation is guaranteed. The proposed design does not allow for on-orbit changes to the program; however, the design could easily be changed to accommodate this should it be desired. The initial design uses external Read/Write Memory (RAM) to augment the microcontrollers internal memory. During the breadboard phase we will examine the memory requirements, in detail, to eliminate external volatile memory if possible.



- NOTES:
1. THESE 2 POLISHED SURFACES: $\left\{ \begin{array}{l} \text{SURFACE QUALITY: 60/40 (SCRATCH/DIG),} \\ \text{FLATNESS: 1 WAVELENGTH PER INCH} \end{array} \right.$
ALL OTHER SURFACES, AS MACHINED.
 2. TOL. ± 0.01 (0.254)
 3. MATERIAL: FUSED SILICA, CORNING 7940 INCLUSION CLASS 0,
HOMOGENEITY GRADE F OR EQUIVALENT.

CERENKOV RADIATOR
FRUSTUM OF PYRAMID WITH FOUR SIDES

Figure 7 Cerenkov Radiator Design.

A watchdog timer provides a measure of CPU fault tolerance by activating the microprocessor's hardware reset if it times out. This provides a means to recover from a Single Event Upset (SEU) event that will induce errors or other anomalous conditions. Part of the flight software housekeeping procedure is to reset the watchdog periodically. If a watchdog timeout occurs, the microcontroller is reset and program operation begins from a known configuration. All watchdog events are reported in the spacecraft digital serial telemetry stream.

The heart of the glue logic needed for microcontroller support will be implemented with a Field Programmable Gate Array (FPGA). A second FPGA should provide the functions of detector pulse latching and counting along with peripheral decoding, watchdog timing,

spacecraft telemetry timing and various housekeeping. Figure 8 shows the functions designed for the Digital Processing FPGA.

2.3 Breadboard Calibration Data Analysis

Analysis of breadboard calibration data were conducted and reported during the Preliminary Design Review (PDR) held at the Phillips Laboratory (Section 2.5). A brief summary of the test results is given below.

2.3.1 Atmospheric Muon Test Results

High energy particles reaching the rear of the quartz radiator provide the largest pulse amplitude when the PMTs are mounted in the rear position. Pulse height resolution for muons with both PMTs in the rear location is about 40%.

2.3.2 Proton Tests at the Harvard Cyclotron

The proton tests verified that the scintillation efficiency of the Cerenkov radiator is very low. High energy protons, above about 130 MeV, will not be counted as electrons because of D3 anti-coincidence processing, and Cerenkov light is only produced by protons above about 350 MeV. The high energy loss in the D1 and D2 SSDs will also help eliminate the low energy protons.

2.3.3 Electron Tests at the RPI Linear Accelerator

The breadboard Cerenkov detector was calibrated with electrons in the energy range of 2.4 MeV to 30.4 MeV. The results indicate that the front PMT location is better for low energy electrons (<10 MeV), while the rear PMT location is better for high energy electrons. Measured electron responses are shown in Figures 9 to 14. Table 3 summarizes the measured detector Areas(0°) for several electron energies, while Table 4 is a summary of the measured Geometric Factors for four electron energies, with PMT1 and PMT2 located at the front of the Cerenkov radiator. In Table 3, note that the nominal D1 and D2 areas are 2.0 cm^2 , but only D1 approaches that value for electrons >10 MeV. Scattering in the Be shield and the D1 and D2 detectors reduces the $A(0^\circ)$ values for D2, D1/D2 coincidence, and for the PMTs. The effective D1/D2 coincidence and PMT $A(0^\circ)$ values are about one fifth of the nominal 2 cm^2 area. In Table 4 the nominal calculated Gf value is $0.044 \text{ cm}^2 \text{ sr}$, but near the threshold of 3 MeV the Gf value for electrons is about one fifth of the calculated value. Above 10 MeV the Gf value for electrons is about two-thirds of the calculated value.

Figure 9 shows the measured Area(0°) for electrons with PMT1/front and PMT2/front, at the near bending magnet. For the PMTs in this position, the pulse amplitude saturates at the highest energies, since the PMTs are located where the light collection efficiency is best for low energy electrons. The near station bending magnet was only suitable for the lower electron energies, since when the last accelerating RF section just before the bending magnet was energized it produced a large amount of bremsstrahlung background in the Cerenkov radiator.

Table 3 Summary of Measured Detector Areas(0°)					
E_e (MeV)	A(D1) (cm ²)	A(D2) (cm ²)	A(D1/D2) (cm ²)	A(PMTs) (cm ²)	PMT1/2 location
2.4	0.69	0.044	0.025	0.020	front/front
4.1	0.89	0.108	0.069	0.063	front/front
7.9	1.17	0.213	0.0116	0.103	front/front
12.7	1.54	0.512	0.267	0.259	front/front
13.7	1.76	0.684	0.316	0.303	front/rear
17.5	1.63	0.593	0.323	0.312	front/front
18.6	1.53	0.630	0.326	0.290	front/rear
26.5	1.55	0.668	0.336	0.329	front/rear
30.4	1.35	0.558	0.287	0.276	front/rear

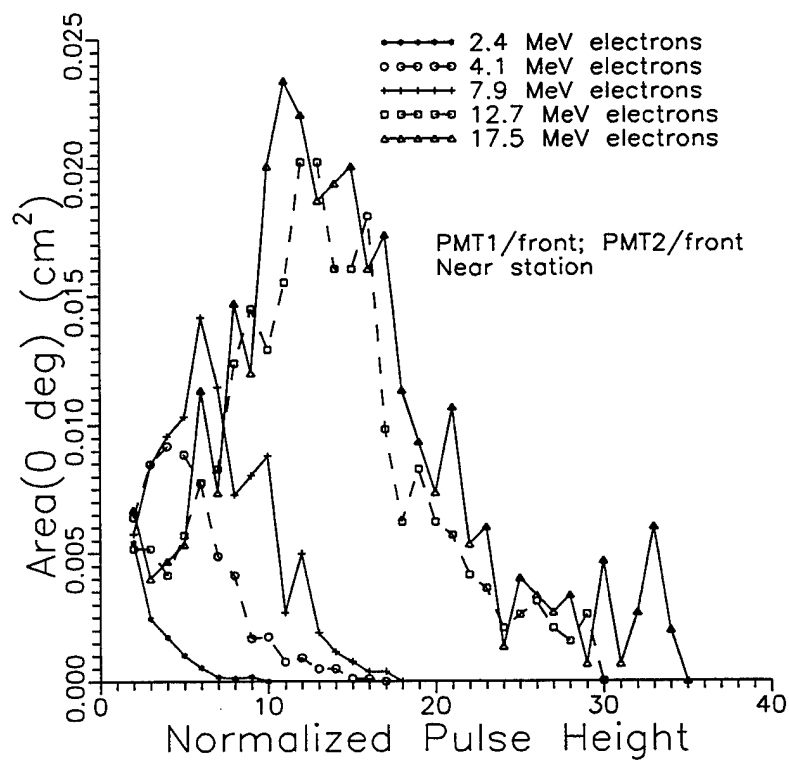


Figure 9 Electron Area(0°) Response, Near Station.

Table 4 Summary of Measured Geometric Factors	
Ee (MeV)	Geometric Factor, Gf (cm ²)
4.1	0.0086
7.9	0.0178
12.7	0.0249
17.5	0.0298

The geometric factors obtained by integrating over the measured angular responses are shown in Figure 10, again for the near bending magnet data. The geometric factors show the same saturation at the high energies, and a low energy tail for all energies.

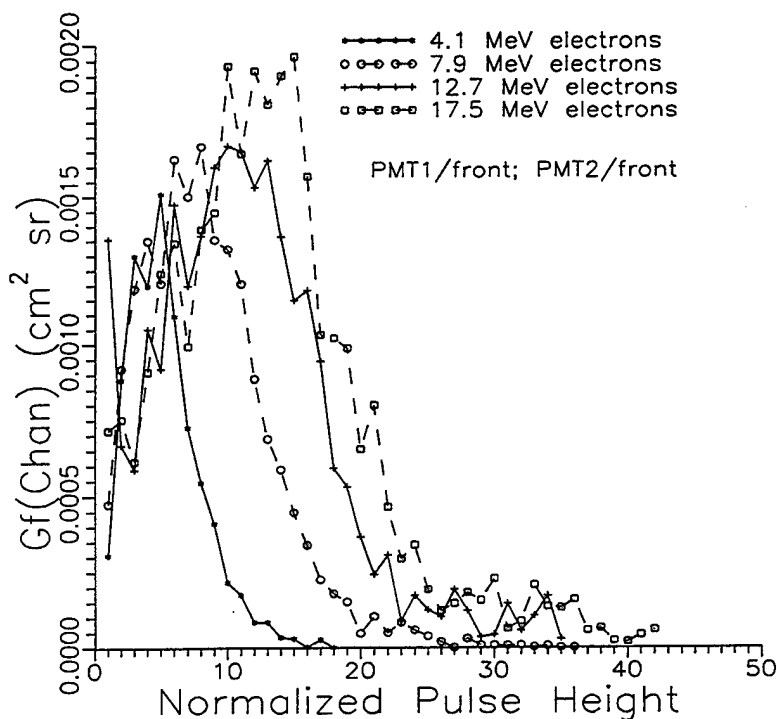


Figure 10 Electron Geometric Factor Response, Near Station.

Figure 11 shows the measured Area(0°) for electrons with PMT1/front and PMT2/rear, at the far bending magnet. This bending magnet location allows the use of electron beams to over 30 MeV without energizing the nearest accelerator RF sections, and thus does not produce an intense bremsstrahlung background in the Cerenkov radiator. The high energy electrons still tend to saturate in pulse height, even with one PMT at the rear of the Cerenkov radiator. The responses also show a low energy tail, which results in integral channels for a differential in pulse height.

The measured Geometric Factors for 12.7 MeV electrons, with PMT1/front and PMT2/front, and PMT1/front and PMT2/rear, are compared in Figure 12. The electrons stop in the front third of the quartz radiator, so the higher amplitude is achieved with both PMTs in front.

The measured Area(0°) for 22.3 MeV electrons, with PMT1/front and PMT2/rear, at the near bending magnet is shown in Figure 13. The different D1 count rates illustrate the "pile-up" effect from the large bremsstrahlung background at the near bending magnet when the accelerator third (nearest) RF section is energized.

The measured response vs. electron energy for three differential channels, using the measured electron geometric factors, are shown in Figure 14. All channels have a strong high energy response, and behave effectively as integral channels above an increasing threshold energy.

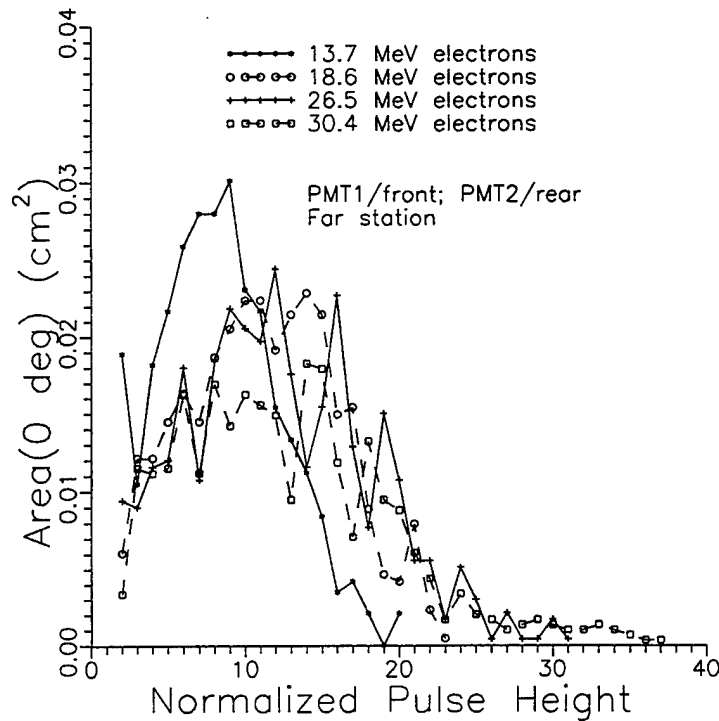


Figure 11 Electron Area Response, Far Station.

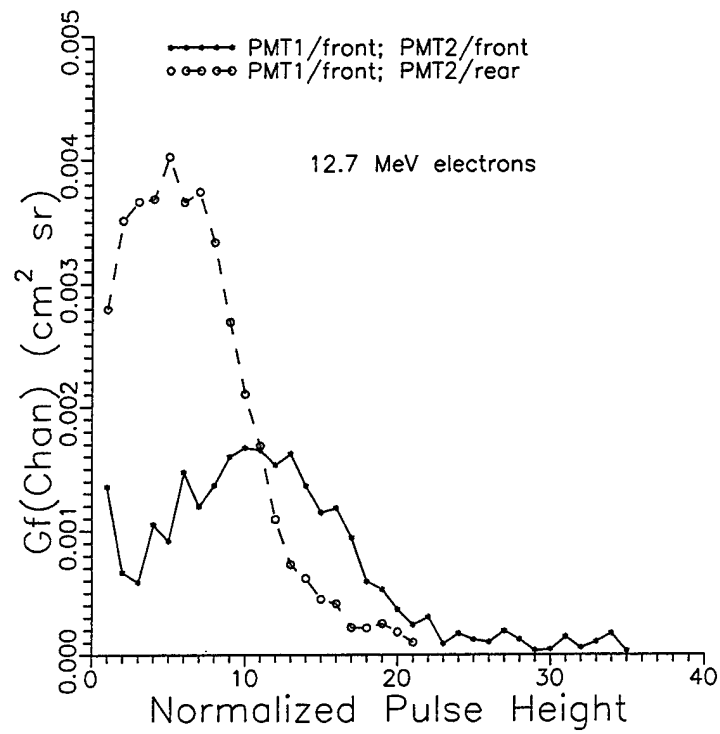


Figure 12 Electron Geometric Factor Response, Far Station.

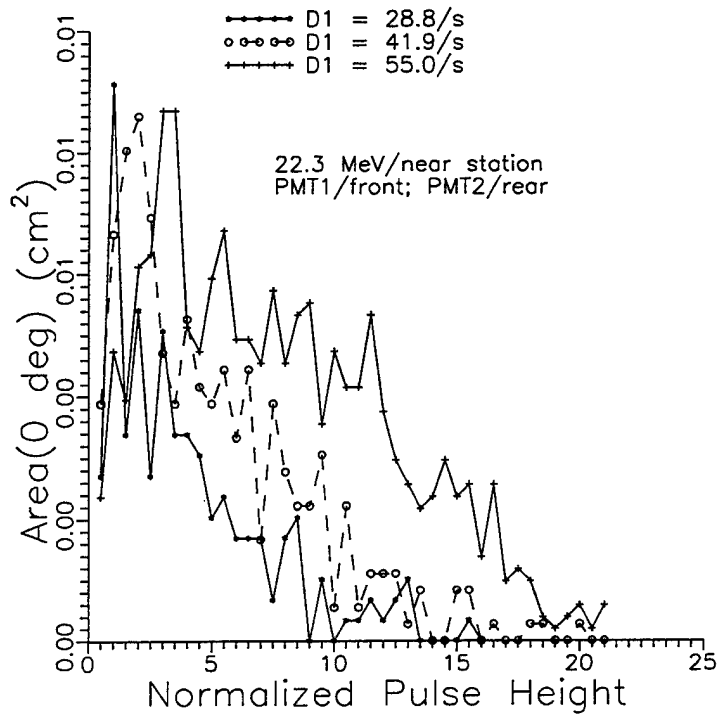


Figure 13 Electron Area Response, with Pile-up at Near Station.

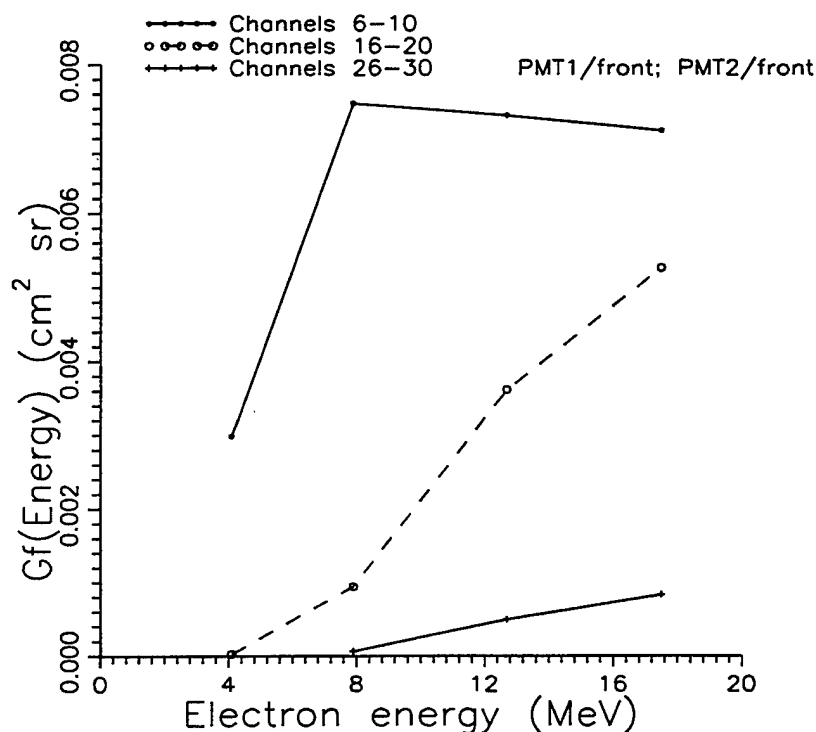


Figure 14 Electron Response vs. Electron Energy.

3.0 Preliminary Design Review

An informal Status Review Meeting was held at the Phillips Laboratory (PL) on November 27, 1995 to review the design status of the spectrometer. The conceptual design was complete and most of the breadboard parts had been ordered. A summary of the initial electronics testing that was underway was given. This was followed by an informal Preliminary Design Review (PDR), held at the Phillips Laboratory (PL) on Thursday, August 1 1996. The electronics design issues discussed are described in Section 3.1, while the discussion of the results of the electron calibration data are summarized in Section 3.2.

3.1 Electronics Design Issues

3.1.1 Low Voltage DC to DC Converter

Initially, the discussions involved tradeoffs of (1) custom converter design or, (2) buying an off-the-shelf converter. Since off-the-shelf, radiation hard, DC to DC Converters are available, the conversion efficiency at the Spectrometer's low power levels is less than it would be with a custom design. It was felt that the DC to DC Converter design problem and cost could be eliminated by using the spacecraft well-regulated ± 5 volt bus. Since other payloads would need the same voltages, it is better to build one converter for the entire group of instruments. The Cerenkov Detector will thus use well regulated ± 5 volt buses provided by the spacecraft. This approach will save on the Spectrometer power and mass.

3.1.2 Standby Power and Power-On Current

The Spectrometer does not need standby power to maintain microcontroller memory or system configuration information. The Spectrometer always powers up in a normal data accumulation mode ready to communicate to SOBEDS. The Spectrometer powers up with the microcontroller executing from high power, rad-hard, bi-polar PROM. The PROM contents are copied to low power Read/Write memory (RAM) then power is removed from the PROM to save power. This design approach was chosen because low power, rad-hard PROMs are not available and rad-hard Electrically Erasable PROMs (EEPROMs) are extremely expensive. Since the spacecraft will be providing the low voltage power for the PROM, it may not be necessary to remove PROM power after turn-on.

3.1.3 Electronic Parts Issues

Many electronic functions will be common to all instruments built for SOBEDS. Proposed electronic parts usage was discussed, and since it is expected that many parts will be common to several instrument designs, PL will review all instrument parts usage. Cost savings should be possible by having a common procurement.

3.2 Measured Electron Energy Resolution

The measured electron responses in Figure 14 show that the Cerenkov Detector response is more a set of integral electron channels, rather than differential channels. This is partly the result of using only two PMTs, and also partly the result of a small Cerenkov radiator, where some high energy electrons scatter (leak) out of the sides and thus generate only a fraction of the full Cerenkov light for an electron which stops in the radiator. The desired response to high energy electrons is for differential channels, since the deconvolving of integral channel responses is less accurate. Thus, the Cerenkov radiator design must be changed, increased in diameter, and additional, larger PMTs must be used to improve the differential channel responses for electrons. This results in a second breadboard radiator design and electron calibration at the RPI Linear Accelerator.

4.0 Sensor Design Status

The electron calibration data from the preliminary Cerenkov radiator design provide the basis for the upgraded design. The new Cerenkov radiator assembly has the following characteristics:

- (1) Larger diameter Cerenkov radiator to allow larger diameter PMTs, and to reduce high energy electron leakage out of the sides of the radiator.
- (2) Cone shaped Radiator, rather than a pyramid.
- (3) Four 38 mm (1.5 inch) PMTs in place of two 25 mm PMTs.

The electronics design has been put on hold until the Cerenkov radiator design has been proven to work properly.

The upgraded Cerenkov Radiator will be designed and assembled with the necessary

detection electronics. This assembly will then be tested at the RPI Linear Accelerator, and the data reduced to geometric factors and differential channel responses. The resulting upgraded responses will be reviewed and the final design selected.

4.1 Analog Signal Processing

The analog processing breadboard electronics that have been designed and built include Charge Sensitive Preamplifiers (CSPAs) the shaping amplifiers and all the threshold detectors. These electronics are ready for the next round of testing at RPI.

4.2 High Voltage Power Supply

The high voltage power supplies were tested during spectrometer calibration and operate satisfactorily, proving out the breadboard design. However, modifications to the current design may be necessary due to the addition of two PMTs.

4.3 Digital Processing

Design of the microcontroller circuitry is currently on hold. However, hardware and software designs are far enough along to report on the design status of the digital processing FPGA (Figure 8) and the proposed spectrometer telemetry format (Table 5).

4.4 Mass, Power and Summary of Characteristics

Table 6 lists a summary of the spectrometer characteristics including mass and power. Both mass and power will change slightly due to the addition of two PMTs and the change in design of the Cerenkov radiator.

4.5 Spacecraft Interface

The spacecraft is expected to provide a +28V Main Bus and $\pm 5V$ logic busses; however, the design may be adjusted to accommodate any bus configuration. Commands and telemetry with the spacecraft are assumed to be similar to that for the APEX spacecraft. The interfacing hardware is expected to be similar to the industry standard RS422 balanced (differential) transmitter/receivers.

5.0 Future Work

The following tasks are planned for the next period:

- 1) Design a new Cerenkov radiator. The current radiator does not have an area large enough for four PMTs to mount so a new radiator will be designed and procured. Also, the breadboard detector assembly will be modified to hold four PMTs along with the extra electronics.
- 2) Procure four 38 mm (1.5 inch) PMTs and build the PMT interface electronics.
- 3) Schedule additional electron testing at RPI.

Table 5 Proposed Spectrometer Telemetry Packet			
Data	Number of Bytes	Data	Number of Bytes
SSD1 LL TH/OS Hardware Counter	3	RAM Counter 11 (445 - 522 MeV p)	2
SSD1 UL TH/OS Hardware Counter	3	RAM Counter 12 (522 - 626 MeV p)	2
SSD2 LL TH/OS Hardware Counter	3	RAM Counter 13 (626 - 812 MeV p)	2
SSD2 UL TH/OS Hardware Counter	2	RAM Counter 14 (812 - 1180 MeV p)	2
PMT TH/OS Hardware Counter	3	RAM Counter 15 (1180 - 2430 MeV p)	2
SSD3 TH/OS Hardware Counter	3	RAM Counter 16 (>2430 MeV p)	2
Fast Coincidence Hardware Counter	2	RAM Counter 17 (Diagnostic count)	2
RAM Counter 1 (3.0 - 4.4 MeV el)	2	RAM Counter 18 (Diagnostic count)	2
RAM Counter 2 (4.4 - 7.8 MeV el)	2	RAM Counter 19 (Diagnostic count)	2
RAM Counter 3 (7.8 - 11.7 MeV el)	2	RAM Counter 20 (Diagnostic count)	2
RAM Counter 4 (11.7 - 15.8 MeV el)	2	RAM Counter 21 (Diagnostic count)	2
RAM Counter 5 (15.8 - 20 MeV el)	2	RAM Counter 22 (Diagnostic count)	2
RAM Counter 6 (20 - 25 MeV el)	2	RAM Counter 23 (Triple Coincidences)	2
RAM Counter 7 (25 - 30 MeV el)	2	Analog Subcommutator	1
RAM Counter 8 (>30 MeV el)	2	Bilevel Subcommutator	1
RAM Counter 9 (371 - 391 MeV p)	2	Cal/Norm Flag and Subcomm Frame Identifier	1
RAM Counter 10 (391 - 445 MeV p)	2	Checksum	2
70 Bytes Total			

Table 6 Spectrometer Summary of Characteristics	
Detectors	3 planar silicon solid state detectors and a Cerenkov radiator with two photo multipliers in a telescope configuration
Field of View	9.5° maximum Field of View (FOV) angle
Energy Ranges	Electrons: 3 MeV to >30 MeV Protons: 371 MeV to >2430 MeV
Output Data Format	560 bits (70 bytes) serial, read once per second, includes commutated analog monitors
Command Requirements	possible: Normal Mode, Calibration Mode, HVPS level (1 of 8), Data Request
Size	11.40 L X 5.80 W X 3.60 H (inches)
Mass	~7 lbs (3.2 kg)
Power	~1.0 W
Temperature Range	0° C to +30° C Nominal Operating -20° C to +35° C Maximum Operating -20° C to +40° C Non Operating
Geometric Factors, Proton	0.044 cm ² sr
Geometric Factors, Electron	0.01 cm ² sr at ~3 MeV ; 0.03 cm ² sr for > 10 MeV

References

1. M. J. Berger and S. M. Seltzer, "Tables of Energy Losses and Ranges of Electrons and Positrons", NASA SP-3012 (1964).
2. M.J.Berger and S.M.Seltzer, "Additional Stopping Power and Range Tables for Protons, Mesons, and Electrons," NASA SP-3036 (1966).
3. J.F.Janni, "Proton Range-Energy Tables, 1 keV - 10 GeV; Part 1. Compounds," Atomic Data and Nuclear Data Tables, 27, No. 2/3, 147-339 (March/May 1982).
4. J.F.Janni, "Proton Range-Energy Tables, 1 keV - 10 GeV; Part 2. Elements," Atomic Data and Nuclear Data Tables, 27, No. 4/5, 341-529 (July/September 1982).
5. A.H.Snell, editor, "Nuclear Instruments and Their Uses," Vol. 1, Wiley, NY (1962).